Cell Death and Differentiation (2016) 23, 1691–1701
© 2016 Macmillan Publishers Limited, part of Springer Nature. All rights reserved 1350-9047/16
www.nature.com/cdd

Astroglial connexin43 contributes to neuronal suffering in a mouse model of Alzheimer's disease

C Yi[1,2,3], X Mei[1,2,3], P Ezan[1,2,3], S Mato[4,5], I Matias[6,7], C Giaume[1,2,3] and A Koulakoff*[,1,2,3]

In Alzheimer's disease (AD), astrocyte properties are modified but their involvement in this pathology is only beginning to be appreciated. The expression of connexins, proteins forming gap junction channels and hemichannels, is increased in astrocytes contacting amyloid plaques in brains of AD patients and APP/PS1 mice. The consequences on their channel functions was investigated in a murine model of familial AD, the $APP_{swe}/PS1_{dE9}$ mice. Whereas gap junctional communication was not affected, we revealed that hemichannels were activated in astrocytes of acute hippocampal slices containing Aβ plaques. Such hemichannel activity was detected in all astrocytes, whatever their distance from amyloid plaques, but with an enhanced activity in the reactive astrocytes contacting amyloid plaques. Connexin43 was the main hemichannel contributor, however, a minor pannexin1 component was also identified in the subpopulation of reactive astrocytes in direct contact with plaques. Distinct regulatory pathways are involved in connexin and pannexin hemichannel activation. Inflammation triggered pannexin hemichannel activity, whereas connexin43 hemichannels were activated by the increase in resting calcium level of astrocytes. Importantly, hemichannel activation led to the release of ATP and glutamate that contributed to maintain a high calcium level in astrocytes placing them in the center of a vicious circle. The astroglial targeted connexin43 gene knocking-out in $APP_{swe}/PS1_{dE9}$ mice allowed to diminish gliotransmitter release and to alleviate neuronal damages, reducing oxidative stress and neuritic dystrophies in hippocampal neurons associated to plaques. Altogether, these data highlight the importance of astroglial hemichannels in AD and suggest that blocking astroglial hemichannel activity in astrocytes could represent an alternative therapeutic strategy in AD.
Cell Death and Differentiation (2016) **23,** 1691–1701; doi:10.1038/cdd.2016.63; published online 8 July 2016

In Alzheimer's disease (AD), the histopathological hallmarks are amyloid-β (Aβ) deposition, neurofibrillary tangles, progressive neuronal suffering and synaptic loss in selective brain areas.[1] An invariant feature is the reactive gliosis associated to Aβ plaques[1] where activated microglia are recruited and astrocytes exhibit a morphofunctional remodeling modifying their interactions with neurons.[2] Indeed, glial cells are increasingly considered as important players in neuropathological processes challenging the neurocentric view of brain diseases,[3–6] but how glial changes contribute to the pathological processes requires further investigation.

In human AD brain[7,8] and murine models of familial AD (FAD),[9] we previously showed that the expression of astroglial connexins (Cxs), Cx30 and Cx43, is increased in the reactive astrocytes surrounding plaques. Cxs are transmembrane proteins forming hemichannels (HCs) which, by docking between adjacent cells, constitute intercellular gap junction channels.[10] The latter underly the astroglial network organization that enables small molecule diffusion to distant cells and contributes to K^+ and glutamate buffering and metabolic trafficking.[11] Interestingly, in two FAD models, gap junctional communication was enhanced or unchanged compared with control mice,[12,13] suggesting that the presence of Aβ has no major impact on signal diffusion within the astroglial network. Cxs can also work as HCs allowing exchanges between the cytoplasm and the extracellular medium.[14] Increasing evidence indicates that HCs formed by Cxs or by another family of proteins, the pannexins (Panx)[15] have important roles in pathological situations.[16–18] HC openings can be triggered in astrocytes after Aβ treatment or in inflammatory situations,[19–22] both occurring in AD. Such activation leads to ATP and glutamate release with neurotoxic effects.[21] Interestingly, Cx43 HCs were proposed as a source of ATP release in a FAD model.[23] Therefore, we asked whether Cx channel functions, noticeably HC function, are impacted in astrocytes of Alzheimer's mice and what are the consequences on neurons.

We have used a FAD model, the $APP_{swe}/PS1_{dE9}$ mice (named APP/PS1),[24] in which we found that gap junctional

[1]Center for Interdisciplinary Research in Biology (CIRB), Collège de France, 75005 Paris, France; [2]Centre National de la Recherche Scientifique Unité Mixte de Recherche 7241, 75005 Paris, France; [3]Institut National de la Santé et de la Recherche Médicale U1050, 75005 Paris, France; [4]Achucarro Basque Center for Neuroscience, Centro de Investigación Biomédica en Red en Enfermedades Neurodegenerativas (CIBERNED), Leioa, Spain; [5]Departamento de Neurociencias, Universidad del Pais Vasco, Leioa, Spain; [6]Institut National de la Santé et de la Recherche Médicale U1215, Neurocentre Magendie, 33077 Bordeaux, France and [7]Université de Bordeaux, 33077 Bordeaux, France
*Corresponding author: A Koulakoff, Center for Interdisciplinary Research in Biology, Collège de France, 11 place Marcelin Berthelot, 75005 Paris, France. Tel: 331442712575; Fax: 33144271268; E-mail: annette.koulakoff@college-de-france.fr

Abbreviations: Aβ, amyloid-β; AD, Alzheimer's disease; APP, amyloid precursor protein; ATP, adenosine triphosphate; CBX, carbenoxolone; Cx, connexin; EtBr, ethidium bromide; FAD, familial Alzheimer's disease; FRAP, fluorescence recovery after photobleaching; GABA, gamma-aminobutyric acid; GFAP, glial fibrillary acidic protein; HC, hemichannel; IL, interleukin; IP3, inositol triphosphate; KO, knock-out; mGluR, metabotropic glutamate receptor; P2, purinergic type2; PanX, pannexin; PKC, protein kinase C; PS1, presenilin-1; RTN3, reticulon 3; RIDN, reticulon 3 immunoreactive dystrophic neurite; sAPPα, soluble amyloid precursor protein alpha; SR101, sulforhodamine-101; TGFβ, transforming growth factor beta; TNFα, tumor necrosis factor α; WT, wild-type

Received 21.3.16; revised 19.5.16; accepted 25.5.16; Edited by N Bazan; published online 08.7.2016

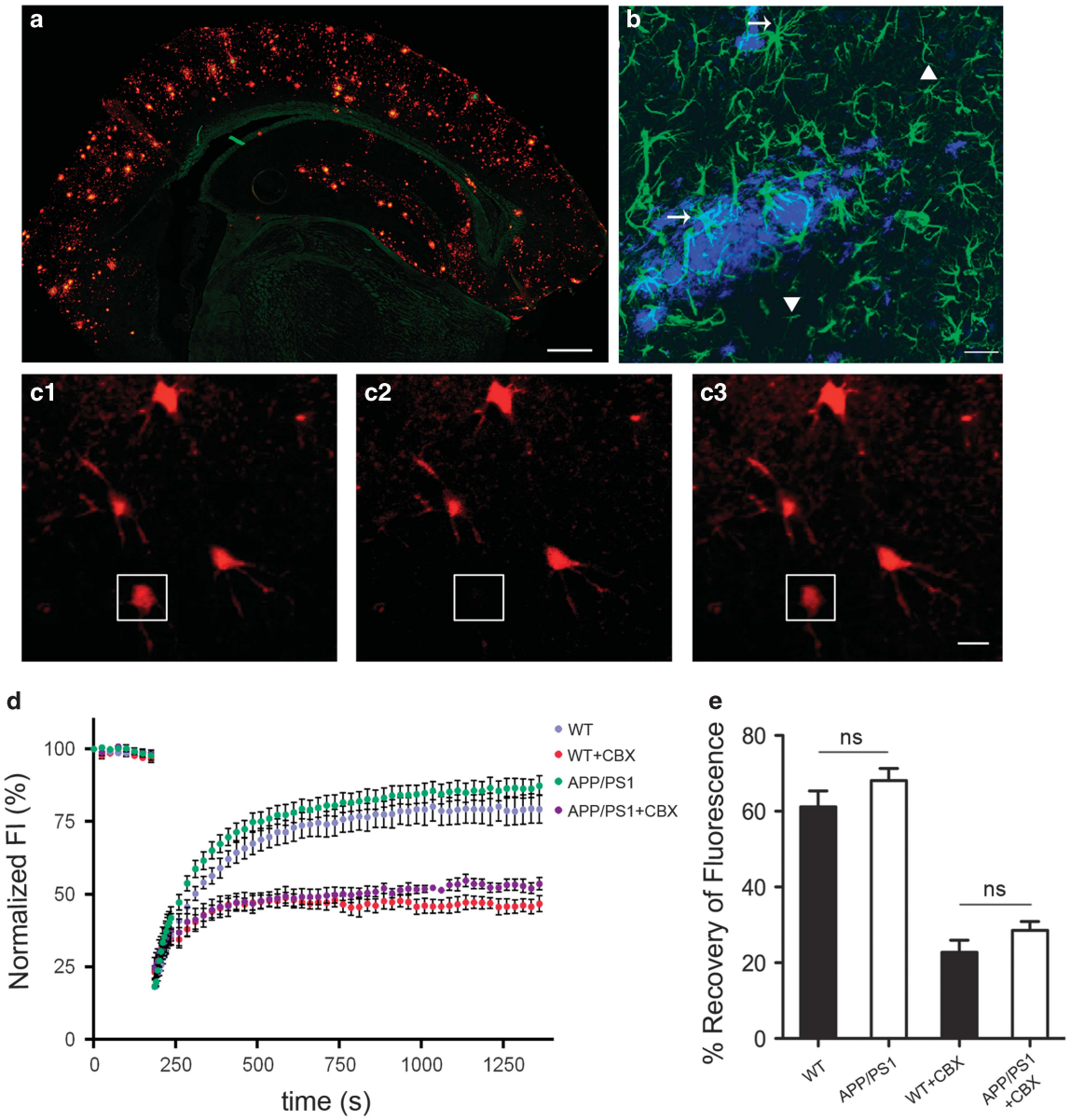

Figure 1 Maintained gap junctional communication in astrocytes of old APP/PS1 mice. (**a**) Distribution of Aβ plaques in brain sections of 9-month-old APP/PS1 mice, stained for Aβ (red) and thioflavine (green); scale bar, 1000 μm. (**b**) Double immunostaining for GFAP (green) and Aβ (blue) of a hippocampal section from 9-month-old APP/PS1 mouse showing the reactive phenotype of astrocytes contacting plaques (white arrow) compared with astrocytes far from plaques (white triangle); scale bar, 30 μm. (**c**) The FRAP technique was used to quantify gap junction function. Images of astrocytes loaded with the gap junction-permeable tracer SR101 before bleaching (**c1**), immediately after bleaching in the white rectangle (**c2**) and 20 min after laser bleach (**c3**); scale bar, 10 μm. (**d** and **e**) Analysis of FRAP in the astrocytes of 9-month-old WT and APP/PS1 mice with or without CBX. (**d**) Time-lapse percentage of fluorescence intensity (FI) normalized with F_0. (**e**) Quantification of fluorescence recovery percentage showing no significant differences between the two genotypes (ns, not significant; unpaired Student's *t*-test; mean $\pm$ S.E.M., WT $n=8$; APP/PS1 $n=9$; WT+CBX $n=7$; APP/PS1+CBX $n=3$)

communication remained similar to that of wild-type (WT) mice and that HCs were chronically activated in all hippocampal astrocytes of mice bearing Aβ plaques. They were predominantly composed of Cx43 whose openings were triggered by high intracellular Ca^{2+} concentration ($[Ca^{2+}]_i$). Pannexin1 was also a minor HC contributer restricted to astrocytes contacting plaques and triggered by inflammation. HC activation contributed to maintain high $[Ca^{2+}]_i$ within astrocytes and allowed for gliotransmitter release that likely led to neuronal suffering. The latter was significantly reduced in APP/PS1 mice with an astroglial Cx43 deletion, opening the way for targeting Cx HCs to alleviate neuronal damages in AD.

Results

Gap junctional communication is not modified in APP/PS1 astrocytes. The APP/PS1 mice used in our experiments accumulate Aβ plaques with age in the cortex and the hippocampus (Figure 1a). The astroglial phenotype differed

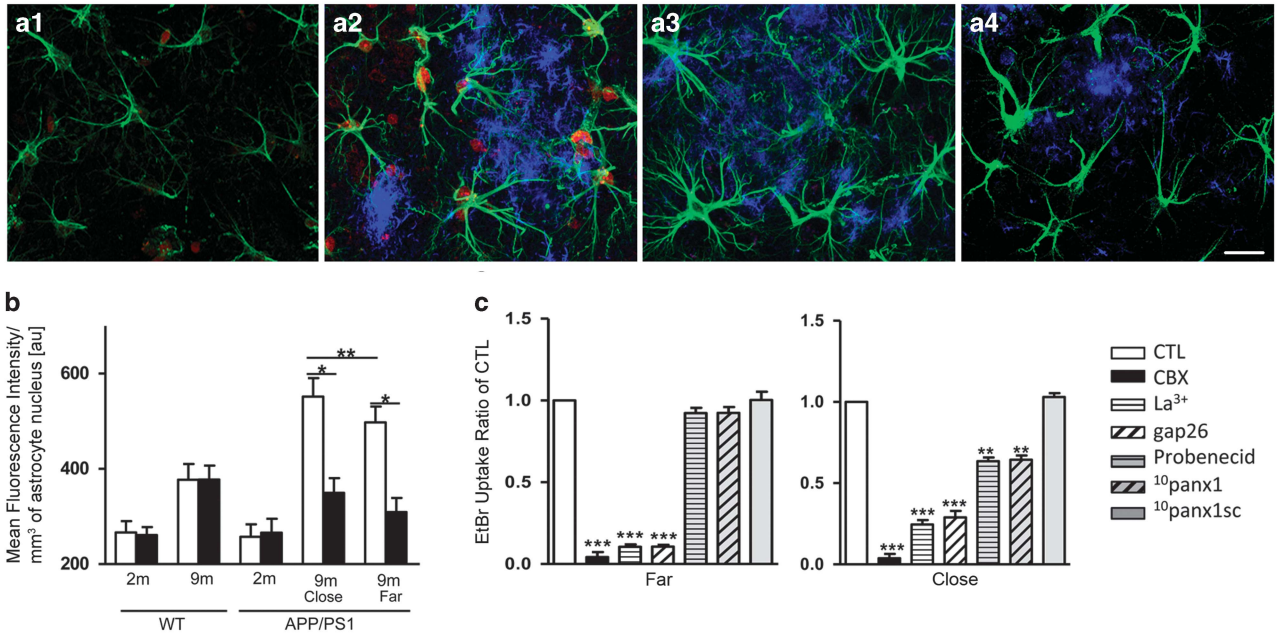

Figure 2 HCs are activated in astrocytes of old APP/PS1 mice. (**a1**–**a4**) EtBr fluorescent signal (red) in hippocampal slices of 9-month-old mice stained for GFAP (green) and Aβ (blue). In WT mice (**a1**), the signal was low compared with the bright signal in APP/PS1 mice (**a2**) that was suppressed by CBX (200 μM) (**a3**) and undetectable when Ethidium homodimer (10 μM) was used (**a4**); scale bar, 30 μm. (**b**) The mean fluorescence intensity of EtBr signal per astrocyte nucleus from WT and APP/PS1 mice measured at the ages indicated is expressed in arbitrary units (au) as mean $\pm$ S.E.M. (*$P<0.05$, **$P<0.01$; Student's *t*-test, $n=5$). (**c**) Histograms showing EtBr uptake in astrocytes far and close to plaques in presence of a series of HC blockers expressed as a ratio of control (CTL) conditions (without blockers) (**$P<0.01$, ***$P<0.001$ *versus* CTL; ANOVA Dunnett's test; mean $\pm$ S.E.M., $n=5$)

according to their proximity to Aβ plaques, allowing to distinguish two populations (Figure 1b): reactive astrocytes contacting plaques with widened processes and enhanced GFAP staining defined as 'close', and astrocytes located at $\geq 50\,\mu$m from plaques, named 'far' that showed neither signs of hypertrophy nor atrophy. We have compared gap junctional communication in hippocampal astrocytes of 9-month-old APP/PS1 and WT mice by using fluorescence recovery after photobleaching (FRAP) on brain slices loaded with SR101, a gap junction-permeant dye selectively taken up by astrocytes (Figure 1c). The kinetics of FRAP in photobleached astrocytes were similar in APP/PS1 and WT mice (Figure 1d) and reached $68.1 \pm 3.2\%$ and $61.1 \pm 4.3\%$, respectively, after 20 min (Figure 1e). In both genotypes, around 40% of this recovery was inhibited by CBX. Moreover, FRAP was similar in astrocytes 'close' and 'far' ($69.0 \pm 4.6\%$ and $70.0 \pm 5.0\%$, respectively), indicating that astroglial gap junctional communication was maintained in APP/PS1 mice and unaffected by the reactive or non-reactive status of astrocytes.

Increased membrane permeabilization in APP/PS1 astrocytes. HC activation was analyzed in acute hippocampal slices using EtBr uptake assay.[25] First, EtBr fluorescent signal in GFAP-stained astrocytes nuclei, taken as an index of uptake, was examined in 9-month-old APP/PS1 and WT mice. This signal was faint in WT mice (Figure 2a1) compared with the bright signal in APP/PS1 mice (Figure 2a2). In the latter, CBX reduced EtBr signal to WT level (Figure 2a3), indicating that most of dye uptake occurred through HCs. In addition, no unspecific uptake due to membrane damage in unhealthy cells was detected by using Ethidium homodimer (Figure 2a4). Then, EtBr fluorescence was quantified in young (2-month-old) and old (9-month-old) mice (Figure 2b). In young WT and APP/PS1 mice without plaques, the fluorescent signal was low and unaffected by CBX. This was also true in old WT mice, although the fluorescent signal was higher. In contrast, in old APP/PS1 mice bearing plaques, EtBr signal was strongly increased in reactive astrocytes contacting plaques (close) and to a lesser extent in non-reactive astrocytes far from plaques (Figure 2b); note that both were reduced to WT levels by CBX, confirming that HCs were activated in astrocytes.

To determine the molecular substrate of HC activity, we have used several HC blockers to discriminate between Cx and pannexin HC contribution[25] and quantified EtBr signal in reactive astrocytes contacting plaques and in non-reactive astrocytes distant from plaques. Carbenoxolone, which blocks both HC families, abolished EtBr uptake in astrocytes, whether 'far' or 'close' (Figure 2c). The pannexin blockers, probenecid and ^{10}panx1, inhibited $36.4 \pm 2.3\%$ and $35.5 \pm 2.6\%$, respectively, of EtBr uptake in astrocytes contacting plaques, but had no effect on astrocytes 'far'. Accordingly, EtBr uptake was strongly reduced by Cx blockers, La^{3+} and Gap26, in astrocytes 'close' (75.4 ± 2.7 and $71.1 \pm 4.0\%$ inhibition) and quite abolished in astrocytes 'far' (89.5 ± 1.5 and $89.5 \pm 1.1\%$ inhibition). We have also examined whether HCs remained activated in older mice (15 months old, Supplementary Figure 1), in which the high plaque load precluded the distinction between close and far astrocytes because most of them contacted plaques and/or small Aβ deposits.

In these cells, EtBr signal was nearly abolished by CBX (97.2 ± 0.6% inhibition), strongly reduced (74.9 ± 6.8 and 75.5 ± 2.5% inhibition) by Cx blockers, La^{3+} ions and Gap26, and partially inhibited (39.5 ± 3.3%) by the pannexin blocker ^{10}panx1. Hence, their EtBr uptake profile was similar to that of reactive astrocytes close to plaques in younger 9-month-old APP/PS1 mice. Altogether, these data show that HCs are activated in all astrocytes of APP/PS1 mice bearing Aβ plaques with a major contribution of Cxs and a minor involvement of Panx1 in astrocytes contacting plaques.

Cx43 is the major contributor to HC activity in APP/PS1 astrocytes. Gap26, which targets Cx43, and La^{3+} ions, which block all Cx HCs, had the same inhibitory effect on HCs in APP/PS1 astrocytes suggesting that Cx43 may be the main Cx involved. To verify this, two colonies of APP/PS1 mice were generated lacking either Cx30 through an ubiquitous deletion or Cx43 through an astrocyte-targeted deletion. EtBr uptake was measured in slices of 9-month-old mice of both genotypes (Figure 3). The pharmacological profile of EtBr uptake was similar in astrocytes from APP/PS1Cx30KO and APP/PS1 mice (Figure 3a): the EtBr signal was reduced by 89.5 ± 8.0% and 64.4 ± 6.8% by Cx blockers in astrocytes 'far' and 'close', respectively. In the latter, 30.9 ± 4.3% of the signal was blocked by ^{10}panx1. These results indicated that Cx30 was not involved in astroglial HC activity in APP/PS1 mice.

In mice lacking Cx43 in astrocytes (APP/PS1Cx43KO), the EtBr signal was hardly detectable in astrocytes 'far', representing 8.4 ± 2.6% of that measured in APP/PS1 astrocytes, confirming the major contribution of Cx43 to the HC activity (Figure 3b). In astrocytes contacting plaques, the low EtBr signal represented 33.1 ± 3.6% of that in APP/PS1 mice and was abolished by CBX or pannexin blockers indicating that it was mediated by Panx1 HCs. The residual EtBr signal detected in astrocytes 'far' was also abolished by CBX and pannexin inhibitors, likely resulting from gap junction-channel-mediated propagation of the EtBr taken up by astrocytes 'close' through Panx1 HCs. Indeed, gap junctional communication was maintained in APP/PS1Cx43KO mice although reduced, compared with APP/PS1 mice (Supplementary Figure 2). Altogether, these data showed that Cx43 HCs were activated in hippocampal astrocytes of APP/PS1 mice whatever their distance to plaques and Panx1 HCs were minor contributors restricted to reactive astrocytes contacting plaques.

Mechanisms underlying HC activation in APP/PS1 astrocytes. To determine whether inflammation triggered HC opening in APP/PS1 astrocytes, brain slices of 9-month-old mice were acutely treated with minocycline that attenuates microglial activation:[26] indeed, microglia exhibited reduced Iba1 immunostaining and lost their activated morphology associated with plaques (Figure 4a). Also, IL-1β content was significantly reduced and TNFα tended to decrease (Figure 4b). EtBr uptake was not affected by minocycline in astrocytes 'far' (Figure 4c) but was reduced by 24.5 ± 2.3% in astrocytes contacting plaques (Figure 4d), suggesting that the anti-inflammatory treatment blocked Panx1 HCs restricted to these astrocytes. This was confirmed by the

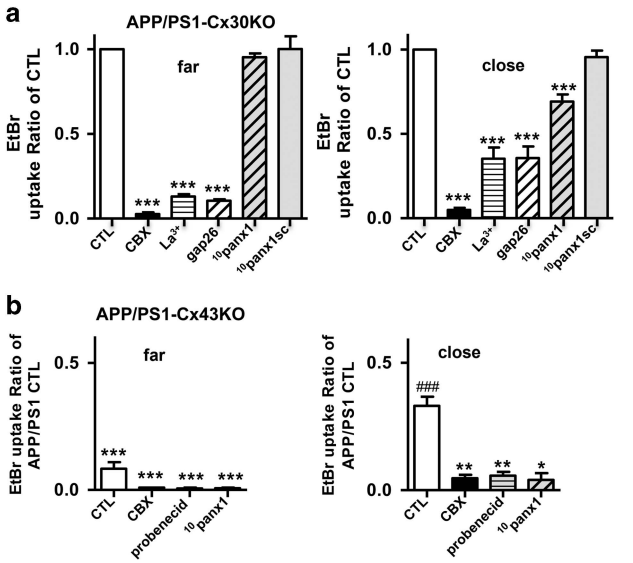

Figure 3 Cx43 is the main component of HCs in astrocytes of APP/PS1 mice. Quantification analysis of EtBr uptake in the presence of indicated HC blockers in astrocytes far (*left*) and close (*right*) to plaques in 9-month-old APP/PS1 mice lacking Cx30 (**a**) or lacking Cx43 in astrocytes (**b**). In (**a**), EtBr uptake is expressed as a ratio of control (CTL) condition without blockers (**$P<0.01$, ***$P<0.001$, *versus* CTL; ANOVA Dunnett's test; mean ± S.E.M., $n=5$). In (**b**), the residual EtBr uptake in APP/PS1Cx43KO mice is expressed as a ratio of values obtained in age-matched APP/PS1 mice in control condition (**$P<0.01$, ***$P<0.001$, *versus* APP/PS1 CTL; ANOVA Dunnett's test; mean ± S.E.M., $n=4$)

absence of additive effect of the Panx1 blocker probenecid in minocycline-treated slices (Figure 4d). Interestingly, similar results were obtained in slices treated by a mixture of IL-1β and TNFα antagonists (Figures 4c and d). These data indicate that inflammation triggered Panx1 HC activity in astrocytes but did not significantly affect Cx43 HCs.

Cx43 HC opening is known to be regulated by $[Ca^{2+}]_i$ and its increase in Cx43-transfected cells resulted in HC activation.[27] Hence, the elevated resting $[Ca^{2+}]_i$ reported in APP/PS1 cortical astrocytes[28] could trigger Cx43 HC activation. First, we confirmed that resting $[Ca^{2+}]_i$ was elevated in APP/PS1 hippocampal astrocytes by comparing the fluorescence intensity of astrocytes in Fluo-4 AM loaded slices of APP/PS1 and WT mice (Figures 5a and b). Then, to determine whether high $[Ca^{2+}]_i$ regulated APP/PS1 astroglial HC activation, slices were treated with BAPTA-AM that decreased $[Ca^{2+}]_i$ under basal level in astrocytes (Figure 5b). In this condition, EtBr uptake was abrogated (Figure 5c). As increased $[Ca^{2+}]_i$ can result from Ca^{2+} release from intracellular stores and/or Ca^{2+} influx through activated membrane receptors, the effect of drugs acting on these two pathways was tested on astroglial $[Ca^{2+}]_i$ in APP/PS1 mice (Figure 5d). Inhibitors of the IP_3 pathway, U73122 and 2-APB, and of ryanodine receptors (dantrolene) significantly reduced $[Ca^{2+}]_i$ towards WT levels. Also, inhibitors of mGluR5 receptors, MPEP or SIB1757, and of P2 purinergic receptors, suramin or PPADS, reduced $[Ca^{2+}]_i$ to the same extent. When HC activity was tested in the presence of each inhibitor, EtBr uptake was quite abolished (≥90% inhibition) in astrocytes 'far' (Figure 5e) and reduced by 70% in reactive astrocytes contacting plaques (Figure 5f). In the latter,

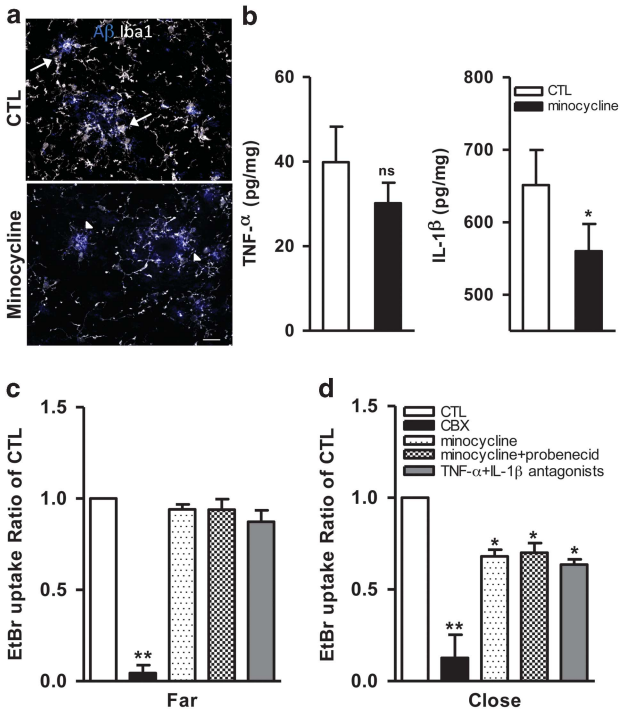

Figure 4 Inflammation triggers Panx HCs. (**a**) Immunostainings for Iba1 (white) and Aβ plaques (blue) of brain hemisphere slices from 9-month-old APP/PS1 maintained 2 h in ACSF alone (CTL) or with minocycline. Scale bar, 20 μm. (**b**) The levels of TNFα and IL-1β measured by ELISA in APP/PS1 slices were reduced after an acute treatment with minocycline (50 nM) during 2 h. (**c** and **d**) Quantification analysis of EtBr uptake in astrocytes far (**c**) and close (**d**) to plaques from APP/PS1 slices treated with the indicated agents. EtBr uptake is expressed as a ratio of control conditions. Anti-inflammatory treatments affected only the astrocytes close to plaques where EtBr uptake was reduced by 30% with no additive effect of Panx blocker (*$P<0.05$, **$P<0.01$, *versus* CTL; ANOVA Dunnett's test; mean $\pm$ S.E.M., $n=5$)

the residual EtBr uptake measured in physiological $[Ca^{2+}]_i$ was abrogated by probenecid or minocycline that prevented Panx1 HC activation (Figure 5g), demonstrating that high $[Ca^{2+}]_i$ triggered Cx43 HCs but not Panx1 HCs.

Altogether, these results indicate that the mechanisms involved in Cx43 *versus* Panx1 HC activation are distinct: high $[Ca^{2+}]_i$ triggers Cx43 HCs whereas inflammatory signals regulate Panx1 HC activity.

HC activity supports Ca^{2+} influx and gliotransmitter release in APP/PS1 mice. Activated HCs allow for Ca^{2+} influx within astrocytes;[22] hence, we have analyzed the effect of HC blockers on astroglial $[Ca^{2+}]_i$ in APP/PS1 mice. Carbenoxolone or Gap26 reduced astroglial $[Ca^{2+}]_i$ to levels close to WT (Figure 6a). Accordingly in APP/PS1Cx43KO, $[Ca^{2+}]_i$ was reduced to the same extent indicating that activated HCs contributed to the increased $[Ca^{2+}]_i$ in APP/PS1 astrocytes.

Also, we examined whether gliotransmitter release resulting of HC activation[14] occurred in APP/PS1 mice. ATP released from brain slices was measured by bioluminescence. The amount of ATP released from APP/PS1 slices (13.7 $\pm$ 1.0 nmol/mg protein) was about twice that from WT (6.1 $\pm$ 1.1 nmol/mg protein) (Figure 6b) and was reduced to WT levels by CBX or Gap26 (6.1 $\pm$ 1.4 and 7.0 $\pm$ 1.0 nmol/mg protein, respectively). The peptide ^{10}panx1 reduced ATP release to a lesser extent (8.5 $\pm$ 1.4 nmol/mg protein). Finally, the amount of ATP released from APP/PS1Cx43KO and WT slices was similar, confirming that activated Cx43 HCs contributed to ATP release in APP/PS1 mice.

L-Glutamate release was evaluated in similar samples by measuring its respective content in the extracellular medium and the slices, then by calculating their ratio as an index of release (Figure 6c). Glutamate release was higher in APP/PS1 than in WT mice and was strongly reduced by CBX (66.7 $\pm$ 15.7%), Gap26 (93.6 $\pm$ 4.9%) and ^{10}panx1 (80.1 $\pm$ 5.5%). The level of glutamate release from APP/PS1Cx43KO mice was reduced (48.5 $\pm$ 15.4%) compared with APP/PS1 mice and returned to WT level.

Finally, contrary to ATP and glutamate, GABA release (Figure 6d) was not significantly affected by CBX or mimetic peptides and was equivalent in all genotypes.

The lack of astroglial Cx43 prevents neuronal damage in APP/PS1 mice. As gliotransmitter release can be neurotoxic, neuronal suffering was compared in 9-month-old APP/PS1 and APP/PS1Cx43KO mice by testing two parameters reflecting neuronal damage. First, the oxidative stress was examined in hippocampal neurons using the mitochondrial superoxide indicator MitoSOX in living slices. A bright fluorescent signal was detected in the pyramidal cell layer of APP/PS1 but not WT mice (Figure 7a), indicating an accumulation of superoxide anions in AD mice neurons as previously reported.[29] In contrast, the MitoSOX signal was hardly detectable in APP/PS1Cx43KO hippocampal neurons like in WT mice (Figure 7b). Interestingly, such reduction of oxidative stress was not observed when APP/PS1 slices were acutely treated with Gap26, indicating that a short-term HC block was not sufficient to reduce neuronal suffering. Second, another characteristic of neuronal damage is the presence of neuritic dystrophies associated with plaques.[1,30] They were examined in brain sections from APP/PS1 and APP/PS1Cx43KO mice immunostained for Aβ and RTN3, a marker of dystrophic neurites in AD.[31] Bright RTN3 immunoreactive bulbous structures typical of dystrophic neurites (RIDNs) were detected within and around plaques in both genotypes. However, in APP/PS1Cx43KO mice, RIDNs were less abundant in large dense core plaques and rarely present in small plaques (Figure 7c). A highly significant reduction (49.4 $\pm$ 1.7%) of RIDNs was found in APP/PS1Cx43KO compared with APP/PS1 mice (Figure 7d). Such reduced neuronal damage occurred although the density and size of Aβ plaques was not significantly different between both genotypes: 290 *versus* 270 plaques/mm^2 of brain area among which 50 *versus* 48 large plaques/mm^2 (diameter $\geq$ 20 mm) in APP/PS1 and APP/PS1Cx43KO mice, respectively (Supplementary Figure 3). Altogether, these observations indicate that the lack of Cx43 in astrocytes and the resultant reduction in HC activity and gliotransmisson significantly attenuate neuronal damage in APP/PS1 mice.

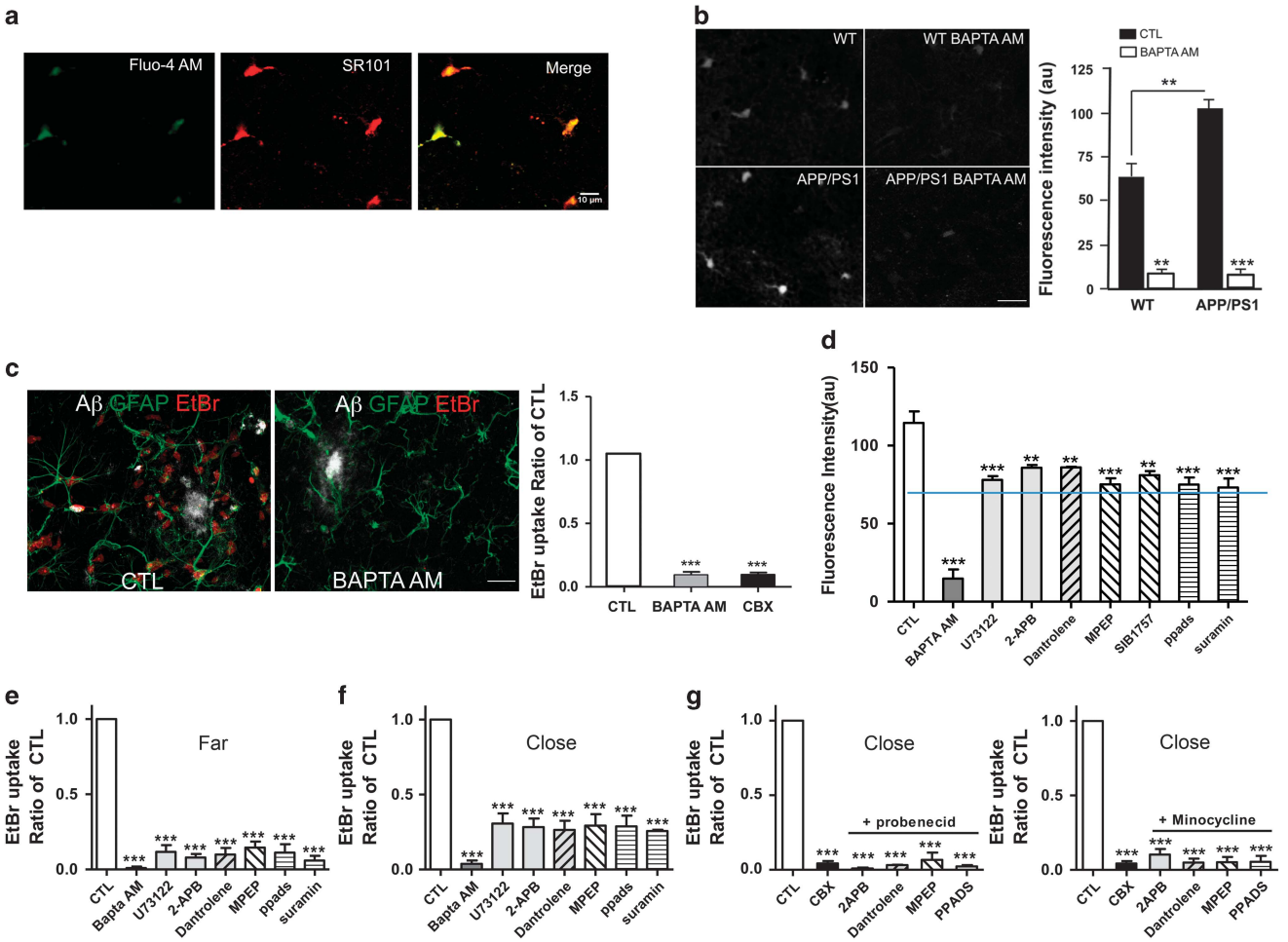

Figure 5 High $[Ca^{2+}]_i$ triggered Cx43 HCs in astrocytes of APP/PS1 mice. (**a**) Images of hippocampal slices of 9-month-old APP/PS1 mice preloaded with Fluo-4 AM (green, left) and labeled with SR101 (red, middle). Merged image (yellow, right) shows that astrocytes selectively loaded Fluo-4 AM. Scale bar, 10 μm. (**b**) Images of Fluo-4 AM fluorescent signal in hippocampal slices of 9-month-old WT and APP/PS1 under control condition (left) or treated 45 min with BAPTA-AM (right). Scale bar, 30 μm. Averaged data of Fluo-4 AM fluorescence levels in astrocytes from WT and APP/PS1 brain slices treated or not with BAPTA-AM expressed in arbitrary units (au) (**$P<0.01$, ***$P<0.001$; Student's *t*-test; mean ± S.E.M., $n=3$) showing that $[Ca^{2+}]_i$ was elevated in APP/PS1 astrocytes and drastically reduced after BAPTA-AM treatment. (**c**) Images of EtBr signal (red) in GFAP-stained astrocytes (green) in brain slices of 9-month-old APP/PS1 mice with Aβ plaques (white) in absence (CTL) or presence of BAPTA-AM. Scale bar, 20 μm. The histogram shows that BAPTA-AM suppressed EtBr uptake as efficiently as CBX (***$P<0.001$, *versus* CTL; Student's *t*-test; values represent the mean ± S.E.M., $n=3$) (**d**) Resting $[Ca^{2+}]_i$ levels expressed as the mean fluorescence intensity of Fluo-4 AM loaded in astrocytes of APP/PS1 brain slices in ACSF alone (CTL) or in presence of the indicated agents. Physiological level in WT mice is indicated by the blue line. (**$P<0.01$, ***$P<0.001$, *versus* CTL; ANOVA Dunnett's test; mean ± S.E.M., $n=3$). (**e–g**) Quantification analysis of EtBr uptake in astrocytes far (**e**) and close (**f** and **g**) to plaques in the presence of these agents to which Panx blocker probenecid (**g**, left) or minocycline was added (**g**, right) that prevented Panx1 HC triggering. In both conditions, EtBr uptake was abrogated in astrocyte-contacting plaques. (***$P<0.001$, *versus* CTL; ANOVA Dunnett's test; mean ± S.E.M., $n=3$)

Discussion

In the present study, we have used a non-aggressive murine model of FAD to examine Cx channel functions in hippocampal astrocytes. Most analyses were performed in 9-month-old mice, when amyloid plaques are scattered enough to analyze Cx functions both in reactive astrocytes contacting plaques and non-reactive astrocytes located far away.

First, we have shown that gap junction channel function was similar in hippocampal astrocytes of APP/PS1 and WT mice, confirming observations reported in other FAD models.[12,13] Interestingly, gap junction-mediated communication was not affected by the proximity of astrocytes to Aβ plaques where clustered activated microglia represent a source of inflammatory cytokines. Such observation contrasts with the reduced gap junctional communication of astrocytes acutely treated with proinflammatory cytokines[19] (but see Abudara *et al.*[22]) or after an *in vivo* inflammatory insult induced by a brain abscess.[20] Interestingly, in the latter situation, gap junctional communication decreased only in the inflammatory nidus but remained normal in regions away from the abscess.

Second, we revealed that Cx43 HCs were chronically activated in hippocampal astrocytes when Aβ plaques are present, whatever their distance from the plaques. However, HC activation was prominent in the astrocytes contacting plaques, which is in line with their higher Cx43 content[7–9] and

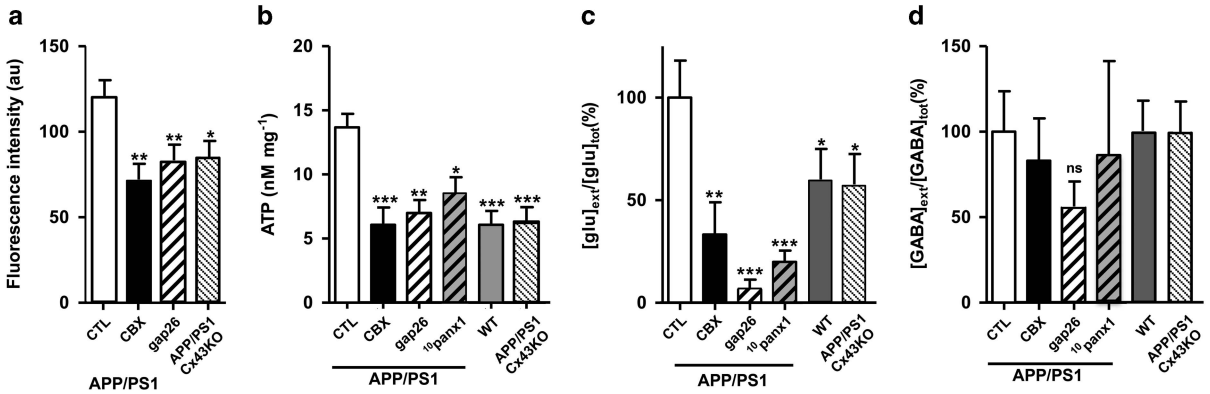

Figure 6 HC activity supports Ca^{2+} influx and gliotransmitter release in APP/PS1 mice. (**a**) Resting $[Ca^{2+}]_i$ levels expressed as mean Fluo-4 AM fluorescence intensity in arbitrary units (au) in astrocytes of APP/PS1 brain hemisphere slices treated or not with CBX or gap26 and from APP/PS1Cx43KO slices under control condition, showing that acute or long-term HC inhibition in APP/PS1 mice decreased $[Ca^{2+}]_i$ (*$P<0.05$, ** $P<0.01$, *versus* APP/PS1 CTL; Student's *t*-test; mean ± S.E.M., $n=3$). (**b–d**) Gliotransmitter levels released from brain hemisphere slices of APP/PS1 (treated or not with HC blockers), WT or APP/PS1Cx43KO mice (ns, not significant, *$P<0.05$, ** $P<0.01$, ***$P<0.001$ *versus* CTL; ANOVA Dunnett's test; mean ± S.E.M., $n=5$). ATP (**b**) and glutamate (**c**) release from APP/PS1 slices were reduced after pretreatment with CBX, gap26, ^{10}panx1 and returned to wild-type level in APP/PS1 mice lacking Cx43. (**d**) GABA release was not significantly affected by HC blockers and was similar in mice of all genotypes

the contribution of Panx1 HCs. Although the issue of the molecular nature of astroglial HCs was highly debated, accumulating evidence indicates that both families of HC-forming proteins can be activated in astrocytes: Cx43 in response to Aβ treatment,[21] ischemia-like conditions[32] or inflammation,[19,33] and Panx1 HCs triggered by P2X7 receptor stimulation, elevated K^+[34] or inflammation.[20] Their relative contribution likely depends on the triggering event, timing after injury or inflammatory context. Our data provide further evidence that the nature of activated HCs in astrocytes depend on their local environment.

In this context, it is worth noting that Cx and pannexin HC activation were driven by different mechanisms in APP/PS1 mice. Inflammatory signals triggered Panx1 HCs solely in astrocytes contacting plaques where activated microglia are concentrated.[30] We cannot exclude that other stimuli in the plaque microenvironment participated in Panx1 HC openings. A local elevation in extracellular K^+ resulting from neuronal hyperexcitability nearby plaques[35] could also promote Panx1 openings as reported in culture.[36] Also, ATP could trigger Panx1 HC openings by activating P2X7 receptors whose expression is increased in reactive glia nearby plaques.[37] In contrast, the main parameter underlying Cx43 HC opening in APP/PS1 mice was the increased $[Ca^{2+}]_i$. Aβ oligomers dysregulate Ca^{2+} homeostasis in astrocytes, especially through increased expression of key components of Ca^{2+} signaling, for example, mGluR5 receptors and IP3R1.[38,39] Hence, treatments that reduced $[Ca^{2+}]_i$, either by blocking pathways of Ca^{2+} release from internal stores or using antagonists of membrane receptors whose activation induces Ca^{2+} increase, led to a concomitant inhibition of Cx43 HC activity.

Interestingly, we have shown that, like in culture[40] or acute slices,[22] Cx43 HCs can also provide a pathway for Ca^{2+} entry in APP/PS1 astrocytes, because astroglial $[Ca^{2+}]_i$ was reduced in brain slices after acute pharmacological Cx43 HC block or in APP/PS1Cx43KO mice. Therefore, a vicious circle takes place in astrocytes in which high $[Ca^{2+}]_i$ triggers Cx43 HC openings that in turn allow Ca^{2+} entry contributing to maintain elevated $[Ca^{2+}]_i$. HC-dependent ATP and glutamate release can amplify this vicious circle by stimulating in an autocrine manner purinergic and glutamatergic metabotropic receptors that contribute also to maintain high $[Ca^{2+}]_i$ in APP/PS1 astrocytes.[28] One consequence of this vicious circle is a chronic Cx43 HC activation leading to gliotransmitter release. Such release can occur directly via HCs, because Cx43 HCs represent a pathway for glutamate release,[41,42] and both Cx[43,44] and Panx HCs can release ATP.[15,34] Indeed, in another FAD model, astroglial Cx HCs were proposed as the source of ATP that triggered P2Y1 receptors leading to increased calcium transients and calcium waves in astrocytes.[23] However, we cannot exclude that other Ca^{2+}-dependent pathways participate in such gliotransmitter release. In contrast, GABA release was not significantly affected in APP/PS1Cx43KO mice confirming that it occurred through a pathway independent of HC activation.[45] The genetic suppression of Cx43 in APP/PS1 astrocytes allowed to reduce $[Ca^{2+}]_i$ as well as extracellular ATP and glutamate levels to WT levels, highly suggesting that the chronic activation of Cx43 HCs sustains this vicious circle in astrocytes.

The chronic gliotransmitter release involving activated HCs can have multiple consequences on neurons, deleterious and/or protective. First, an excess of extracellular glutamate could act on neuronal NMDA receptors, in particular extrasynaptic receptors, and contribute to dysregulate neuronal Ca^{2+} homeostasis and promote synaptic loss.[46] Neuronal Ca^{2+} overload has numerous downstream deleterious consequences including structural neuritic alterations[47] and increased oxidative stress, occurring early in AD.[48] Indeed, in APP/PS1 mice, oxidative stress was triggered in dystrophic neurites nearby plaques and propagated into the cell body leading to caspase-dependent death in some vulnerable cortical neurons.[49] Second, an excess of ATP can also stimulate ionotropic (P2X) and metabotropic (P2Y) receptors that mediate multiple functions in brain cells. By activating P2X7 receptors in astrocytes and microglia, ATP could favor the rapid release of IL-1β, which is potentially neurotoxic.[50] It might also act directly on neuronal purinergic receptors

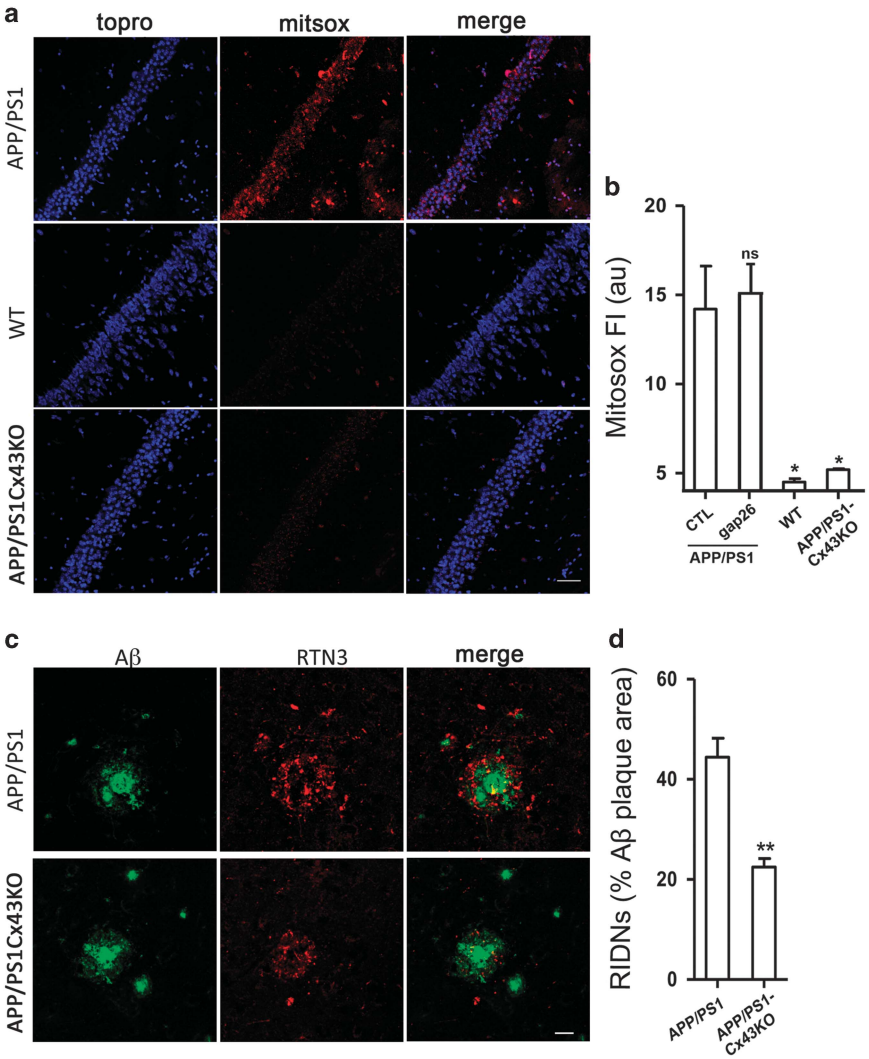

Figure 7 Reduced neuronal damage in APP/PS1 mice lacking astroglial Cx43. (**a**) Images of TO-PRO staining (blue) and MitoSOX signal (red) in the hippocampal pyramidal cell layer of mice of the indicated genotypes showing that the level of mitochondrial superoxide was high in APP/PS1 compared with WT and APP/PS1Cx43KO mice. Scale bar, 50 μm. (**b**) Quantification of the mean fluorescence intensity of MitoSOX in the pyramidal cell layer of indicated genotypes indicating that the lack of Cx43 in APP/PS1 mice reduced the mitochondrial superoxide level to WT levels while an acute treatment of APP/PS1 slices with a Cx43 mimetic peptide had no effect (*$P<0.05$; Student's *t*-test; mean $\pm$ S.E.M., $n=3$). (**c**) Images of immunostainings for Aβ plaques (green) and RTN3 (red) in hippocampal sections from APP/PS1 and APP/PS1Cx43KO mice. RTN3 labeled dystrophic neurites appeared as bright red dots concentrated in and around Aβ plaques and were less abundant in APP/PS1Cx43KO mice. Scale bar, 30 μm. (**d**) The histogram shows that the area occupied by RTN3 stained dystrophic neurites in Aβ plaques was significantly smaller in APP/PS1Cx43KO *versus* APP/PS1 mice (**$P<0.01$; unpaired Student's *t*-test; mean $\pm$ S.E.M., $n=5$)

leading to neuronal Ca^{2+} overload with its cascade of detrimental outcome. The lack of astroglial Cx43 in APP/PS1Cx43KO mice contributes to reduce oxidative stress and neuritic dystrophies in hippocampal neurons likely by tuning down glutamate and ATP release.

However, in the APP/PS1 mice used, no overt neuronal loss was reported except in few cortical neurons.[49] This suggests that, despite elevated ATP and glutamate levels, compensatory neuroprotective mechanisms take place to prevent neuronal death. Pleiotropic neuroprotective effects of ATP were reported upon P2Y receptor activation.[51] For example, astroglial P2Y1 receptor activation can induce the release of the neuroprotective IL-6,[52] while P2Y2 receptor activation can trigger α-secretase and promote growth factor release and APP cleavage towards a soluble neuroprotective ectodomain sAPPα.[53] P2X7 receptor activation can also promote sAPPs formation.[54] In addition, ATP can convert into adenosine whose binding to A1 receptors stimulates PKC and increases sAPPα formation. Finally, glutamate also can sustain neuronal survival by triggering mGluR3 receptors leading to the release of the neuroprotective TGFβ and of sAPPα.[55] Consequently, there is likely a balance between prosurvival and prodeath signaling in neurons that mitigates the neurodegenerative processes and prevents the last steps of neurotoxicity leading to death.

In conclusion, in FAD mice, functional changes in astrocytes can affect their interactions with neurons. The chronic activation of astroglial HCs shown here contributes to maintain

a high $[Ca^{2+}]_i$ in astrocytes that allows a sustained gliotransmitter release, which posit astrocytes as amplifiers of toxicity that participate with other actors in neuronal injury. The lack of Cx43 in astrocytes significantly reduces neuronal suffering in APP/PS1 mice. Cx43 HCs being accessible via the extracellular medium may represent interesting targets to design tools susceptible to alleviate neuronal damages.

Materials and Methods

Animals. $APP_{swe}/PS1^{24}_{dE9}$ and C57Bl/6 mice were obtained from Jackson Laboratories (Bar Harbor, ME, USA); $APP_{swe}/PS1_{dE9}$ Cx30 − / − mice and $APP_{swe}/PS1_{dE9}$-Cx43fl/fl-GFAP/cre mice were generated in the SPF animal facility of the Collège de France by crossbreedings $APP_{swe}/PS1_{dE9}$ with Cx30 − / − and GFAP-creCx43fl/fl, respectively. Experiments were performed on mice of either sex according to the European Community Council Directives (2010/63/UE).

Acute brain slices. Acute brain hemisphere slices (300 μm) were cut on a vibroslicer and transferred to a holding chamber where they rested on a nylon mesh, submerged in oxygenated artificial cerebrospinal fluid (ACSF) at room temperature (RT) for a stabilization period of 60 min. The ACSF solution contained (in mM): NaCl (125); KCl (2.5); $NaHCO_3$ (25); NaH_2PO_4 (1.25); glucose (25); $MgCl_2$ (1); $CaCl_2$ (2).

Dye uptake in acute brain slices. Acute slices were incubated with the HC-permeable fluorescent tracer Ethidium bromide (EtBr, Sigma-Aldrich, St Quentin Fallavier, France) for 10 min at 4 μM final concentration at RT. To determine the sensitivity of EtBr uptake to Cx or pannexin HCs blockers, slices were preincubated in ACSF supplemented with each blocker during 15 min prior to dye application. The blockers used were: carbenoxolone (CBX, 200 μM), La^{3+} ions (400 μM), probenecid (1 mM) or mimetic peptides targeting Cx43 or pannexin1, Gap26 (0.3 mg/ml) and ^{10}panx1 (0.5 mg/ml), respectively, and pannexin1 scrambled peptide (0.5 mg/ml) for control. Following EtBr incubation, slices were rinsed three times in ACSF, fixed for 1 h in 4% paraformaldehyde and processed for immunostainings.

Fixed slices were preincubated in PBS containing 0.2% gelatin and 1% Triton-X100 (PBS*) for 30 min two times, and then incubated overnight at 4 °C in primary antibodies diluted in PBS*. Mouse or chicken antibodies anti-GFAP (1:500, Sigma-Aldrich and ABCAM, Cambridge, UK), rabbit anti-Aβ (1:1000, Life Technologies, Thermo-scientific, France) and rabbit or goat anti-Iba1 (1:500, Wako, Neuss, Germany) were used to detect astrocytes, Aβ deposits and microglia, respectively. After 2 × 30 min washes in PBS*, sections were incubated for 2 h at RT with a mixture of Alexa-conjugated appropriate secondary antibodies (diluted in PBS* 1:2000, Molecular Probes, Eugene, OR, USA), washed and mounted in Fluoromount (Southern Biotechnology, Birmingham, AL, USA). These slices were examined at × 40 with a confocal laser scanning microscope SP5, (Leica, Wetzlar, Germany). Four images covering CA1 to CA3 hippocampus were captured for each experimental condition. Stacks of 22 consecutive confocal images taken at 0.5-μm intervals were acquired sequentially with three lasers (argon 488 nm, 561 nm for EtBr and 647 nm).

EtBr fluorescent signal in astrocyte nuclei was analyzed using Mac Imaris 7.4.0 software. Cells that satisfied the following criteria were considered as $EtBr^+$ astrocytes: (i) cells positive for GFAP; (ii) cells whose nuclei exhibited EtBr fluorescence intensity above the threshold defined in areas outside nuclei and (iii) cells whose nuclei volume was > 100 μm^3 (diameter ≥ 6 μm) to eliminate incomplete objects. Counts were carried out for 200 cells per condition. First, the percentage of $EtBr^+$ astrocytes was calculated among the population of $GFAP^+$ cells. Then, the fluorescence intensity per nucleus and the volume of the nuclei of $EtBr^+$ astrocytes were measured. The mean fluorescence intensity of the population of $EtBr^+$ astrocytes per experimental condition was then calculated. EtBr uptake for each condition was determined by taking into account the percentage of $EtBr^+$ astrocytes and their mean fluorescence intensity. Finally, the EtBr uptake ratio in each condition was normalized to the control condition.

Fluorescence recovery after photobleaching (FRAP). To evaluate gap junction function, we have used FRAP to measure cell-to-cell exchange of a fluorescent diffusion tracer,[25,56] sulforhodamine-101 (SR101) that is selectively taken up by astrocytes and passes through gap junctional channels.[57] Acute brain hemisphere slices of 9-month-old WT, APP/PS1 and APP/PS1Cx43KO mice were prepared as described above. They were then incubated in 1 μM SR101 at 37 °C for 30 min. After 20 min wash in ACSF, the slices were placed in the stage of a confocal microscope and perfused with oxygenated ACSF during the whole experiment. Acquisitions were performed using a Leica × 25, NA = 0.95, water immersion objective on a Leica SP5 MP microscope controlled by the Leica Acquisition Software. After excitation with the 561 nm line of laser, a baseline fluorescence was collected every 25 s during 200 s. Then, the laser scanning was restricted to a square (15 μm × 15 μm) covering the whole cell body of the target astrocyte with a zoom × 3. Fifteen pulses of light at full power of the laser were applied to bleach this target area. Then, the normal recording configuration was reestablished and fluorescence recovery was recorded every 25 s during 20 min. Images were analyzed offline: the mean fluorescence intensity of astrocyte cell body was measured with Image J software. F_0 was regarded as the first value of the baseline recording. The fluorescence intensity of each timepoint was normalized to F_0 and then expressed as percentage of F_0 (F_t/F_0%). The percentage of recovery was calculated by using the plateau value (the average of the last six values of the recording) subtracting the value of the first time point after photobleaching. All studies were performed at 45 μm below the surface to ensure that the cells of interest had not been damaged during preparation. Carbenoxolone, which inhibits gap junction channels, was used as a negative control in these experiments.

TNFα and IL-1β measurements by ELISA. Brain hemisphere slices from 9-month-old APP/PS1 mice (300 μm, two slices for each condition) were treated or not with minocycline (50 nM, Sigma-Aldrich) during 2 h, transferred into tubes, frozen and stored at − 80 °C until processing. Slices were immersed in ice-cold lysis buffer containing (in mM) Tris-HCl 50, NaCl 100, EDTA 2, 1% Triton-X100 and 1% protease inhibitor cocktail (Sigma-Aldrich), and sonicated for 10 s. Samples were centrifuged at 13 200 r.p.m. for 20 min at 4 °C and supernatants stored at − 80 °C. A BCA kit (Thermo Scientific, France) was used for protein determination. Levels of TNFα and IL-1β in these samples were measured using ELISA kits (Invitrogen, Thermo-scientific, France) according to the manufacturer's protocol.

Calcium imaging. Acute brain hemisphere slices from 9-month-old mice were incubated for 60 min at 37 °C in ACSF containing 0.02% Pluronic F-127 and Fluo-4 AM (5 μM, Molecular Probes), a calcium indicator specifically loaded in astrocytes.[58] In some experiments, astrocytes were also identified by their ability to take in SR101. For that, acute slices were incubated for 20 min at 34 °C in ACSF solution containing 1 μM SR101, washed and processed as above for Fluo-4 AM loading. Fluo-4 AM-loaded slices were further treated with different agents separately: BAPTA-AM (25 μM) during 45 min, and antagonists of phospholipase C (U73122, 5 μM, Tocris, Bristol, UK), IP3R (2-APB, 100 μM, Tocris), Ryanodine receptor (RyR) (dantrolene, 30 μM, Tocris), mGluR5 (MPEP 10 μM and SIB1757 50 μM, Tocris) and purinergic receptors (PPADS 100 μM and suramin 100 μM, Tocris) during 30 min. Then, slices were transferred on the stage of a two-photon microscope and Ca^{2+} measurements were carried out. Fluo-4 AM was excited at 910 nm, using a pulsed Maitai (Spectra Physics, Evry, France) laser. Emitted fluorescence was detected using two non-descanned detectors, with a 525/50 nm filter. Acquisitions were carried out with a Leica × 25, NA = 0.95, water immersion objective (with a zoom × 1.5) on a Leica SP5 MP microscope controlled by the Leica Acquisition Software. When SR101 was used, it was excited at 760 nm and the emitted fluorescence was detected using a 585/40 nm filter. Images were analyzed offline: the mean fluorescence intensity of astrocyte soma reflecting the resting Ca^{2+} level was measured with Image J software.

Determination of L-glutamate and GABA levels by commercial laser-induced fluorescence capillary electrophoresis. Extracellular levels of L-glutamate and GABA were determined from acute brain hemisphere slices of 9-month-old mice (two slices/tube/condition, in five mice per genotype) incubated in 1 ml oxygenated ACSF as described.[59] Slices were treated with HC blockers during 150 min; samples of extracellular medium were collected, directly frozen in liquid nitrogen and stored at − 80 °C. Intracellular levels of L-glutamate and GABA in slices were also analyzed. Briefly, pooled slices were deproteinized by addition of cold trichloroacetic acid to a 5% final concentration. The suspension was centrifuged at 16 800 × *g* for 10 min; the trichloroacetic acid was extracted from the supernatant with water-saturated diethyl ether and stored at − 80 °C. Samples were analyzed with a commercial laser-induced fluorescence capillary electrophoresis (capillary electrophoresis: Beckman Coulter (Villepinte, France), P/ACE MDQ; laser-induced fluorescence: Picometrics (Labège, France), LIF-UV-02, 410 nm 20 mW) as following: samples were processed for micellar commercial laser-induced fluorescence capillary electrophoresis and were fluorescently derivatized at RT for

60 min with napthalene-2,3-dicarboxaldehyde before being analyzed by CE using a hydroxypropyl-β-cyclodextrin based chiral separation buffer. All electropherogram data were collected and analyzed using Karat 32 software v8.0 (Beckman Coulter). Further analysis was made using GraphPad Prism 4.03 software.

The extracellular and intracellular amounts of L-glutamate and GABA were normalized to the protein content determined from pooled slices using the BCA kit. The quantity of L-glutamate and GABA in the samples was determined from a standardized curve while peak identification was made by spiking the fraction with the amino acid. For accurate comparison between conditions, extracellular levels of L-glutamate (referred as $[glut]_{ext}$) were normalized to total L-glutamate (intracellular+extracellular) (referred as $[glut]_{tot}$) allowing to assess the released fraction of L-glutamate. $[GABA]_{ext}$ was also normalized to $[GABA]_{tot}$.

Determination of ATP extracellular levels by bioluminescence. Extracellular levels of ATP were determined from acute brain hemisphere slices of 9-month-old mice (two slices/tube/condition, five mice per genotype) incubated in 1 ml oxygenated ACSF. After equilibration, slices were treated or not with HC blockers during 30 min in the presence of an ectonucleotidase inhibitor, 6-*N,N*-diethyl-β-γ-dibromomethylene-D-adenosine-5-triphosphate FPL 67156 (ARL 67156 trisodium salt, Tocris) to inhibit ATP hydrolysis. Then, samples of extracellular medium were collected and extracellular ATP was directly measured using the luciferin-luciferase bioluminescent assay (ATPLite kit, Perkin Elmer, Waltham, MA, USA). Each condition was run in triplicate. Luminescence was measured using a luminometer (Berthold Technologies, Thoiry, France) according to the manufacturer's instructions. The extracellular ATP was normalized to the protein content determined from pooled brain slices by BCA kit (as above).

Immunohistochemical stainings. Cryostat sections (15 μm) prepared as previously described[9] were fixed 30 min at RT with 4% paraformaldehyde, washed in PBS, treated 10 min with 70% formic acid (when mouse anti-Aβ clone 4G8 wad used) and preincubated in PBS containing 0.2% gelatin and 0.25% Triton-X100 (PBS**) for 30 min. Sections were then processed for immunostaining by overnight incubation at 4 °C with primary antibodies including rabbit anti-Aβ (1:1000, Life Technologies) and mouse anti-GFAP (1:500, Sigma-Aldrich) or mouse anti-Aβ (clone 4G8, 1:500) and rabbit anti-RTN3 (R458, 1:1000) diluted in PBS**, washed in PBS** and incubated in secondary goat anti-rabbit and anti-mouse IgG antibodies conjugated with different Alexa FluoR (Molecular Probes) diluted 1:2000 in PBS**. Sections were washed, mounted in Fluoromount and examined with a confocal microscope.

Quantification of RTN3 immunoreactive dystrophic neurites. RTN3 immunoreactive dystrophic neurites (RIDNs) were quantified as previously described with slight modifications:[60] stacks of 30 consecutive optical sections (0.5 μm each) were captured with a $\times$40 objective and Z maximal projections reconstructed with the Leica software. For each mouse (four age-matched mice per genotype were used), six brain sections every 120 μm were stained and quantified. In each brain section, four maximal projection images were captured randomly in the cortex and hippocampus. Image J Software was used to quantify the area of RIDNs at the level of Aβ plaques. Typically, the signals of RIDNs were bright, while cell staining by RTN3 antibodies was dim. RIDNs contained within Aβ plaque areas were selected for quantification. Percentage of RIDNs area was calculated by dividing the total RIDNs area by the total area occupied by Aβ plaques in each mouse.

Detection of mitochondrial superoxide in acute brain slices. Living brain hemisphere slices from 9-month-old mice were incubated with MitoSOX Red, a mitochondrial superoxide indicator (Life Technologies), 5 μM in ACSF for 10 min. Slices were then fixed with 4% paraformaldehyde at 4 °C for 1 h. After washing and permeabilization in PBS*, slices were further incubated with TO-PRO-3 Iodide (diluted in PBS* 1:2000, Life Technologies) at RT for 10 min, rinsed and mounted onto slides with fluoromount. The slices were examined using a Leica SP5 confocal microscope with a $\times$40 objective. Stacks of 22 consecutive confocal images taken at 0.5-μm intervals were acquired sequentially with two lasers (561 nm for MitoSOX and 647 nm for TO-PRO). All parameters were held constant for all the sections. Four images covering the pyramidal layer visualized with TO-PRO nuclear staining in CA1 hippocampal formation were captured for each mouse (three age-matched mice per genotype). Image J Software was used to quantify the mean fluorescence intensity in the pyramidal cell layer.

Statistical analysis. Values are presented as mean $\pm$ S.E.M.; *n* corresponding to the number of independent experiments. Statistical analysis was performed on raw data with Graphpad software using one-way analysis of variance followed by Dunnett's test or via a two-tailed Student's *t*-test. The level of significance was set at $P < 0.05$. Graphics were prepared using GraphPad prism (Northampton, MA, USA).

Conflict of Interest

The authors declare no conflict of interest.

Acknowledgements. We thank E Amigou and J Lelovski for technical help, J Teillon for confocal image analysis training, the animal facility staff and Prof R Yan for the gift of anti-RTN3 antibodies. C YI was supported by FRM. This study was funded by LECMA, CRPCEN, MINECO/FEDER (Grant SAF2013-45084- R) and CIBERNED (Grant PRY-15-404).

Author contributions

AK wrote the manuscript; CY, AK and CG designed the research; CY, XM, PE, SM and IM performed the research; CY analyzed the data.

1. Selkoe DJ. Cell biology of the amyloid beta-protein precursor and the mechanism of Alzheimer's disease. *Annu Rev Cell Biol* 1994; **10**: 373–403.
2. Sofroniew MV, Vinters HV. Astrocytes: biology and pathology. *Acta Neuropathol* 2010; **119**: 7–35.
3. Giaume C, Kirchhoff F, Matute C, Reichenbach A, Verkhratsky A. Glia: the fulcrum of brain diseases. *Cell Death Differ* 2007; **14**: 1324–1335.
4. Verkhratsky A, Olabarria M, Noristani HN, Yeh CY, Rodriguez JJ. Astrocytes in Alzheimer's disease. *Neurotherapeutics* **7**: 399–412.
5. Parpura V, Heneka MT, Montana V, Oliet SH, Schousboe A, Haydon PG *et al.* Glial cells in (patho)physiology. *J Neurochem* 2012; **121**: 4–27.
6. Pekny M, Pekna M, Messing A, Steinhauser C, Lee JM, Parpura V *et al.* Astrocytes: a central element in neurological diseases. *Acta Neuropathol* 2016; **131**: 323–345.
7. Nagy JI, Li W, Hertzberg EL, Marotta CA. Elevated connexin43 immunoreactivity at sites of amyloid plaques in Alzheimer's disease. *Brain Res* 1996; **717**: 173–178.
8. Koulakoff A, Mei X, Orellana JA, Saez JC, Giaume C. Glial connexin expression and function in the context of Alzheimer's disease. *Biochim Biophys Acta* 2012; **1818**: 2048–2057.
9. Mei X, Ezan P, Giaume C, Koulakoff A. Astroglial connexin immunoreactivity is specifically altered at beta-amyloid plaques in beta-amyloid precursor protein/presenilin1 mice. *Neuroscience* 2010; **171**: 92–105.
10. Giaume C, Koulakoff A, Roux L, Holcman D, Rouach N. Astroglial networks: a step further in neuroglial and gliovascular interactions. *Nat Rev Neurosci* 2010; **11**: 87–99.
11. Rouach N, Koulakoff A, Abudara V, Willecke K, Giaume C. Astroglial metabolic networks sustain hippocampal synaptic transmission. *Science* 2008; **322**: 1551–1555.
12. Cruz NF, Ball KK, Dienel GA. Astrocytic gap junctional communication is reduced in amyloid-beta-treated cultured astrocytes, but not in Alzheimer's disease transgenic mice. *ASN Neuro* 2010; **2**: e00041.
13. Peters O, Schipke CG, Philipps A, Haas B, Pannasch U, Wang LP *et al.* Astrocyte function is modified by Alzheimer's disease-like pathology in aged mice. *J Alzheimers Dis* 2009; **18**: 177–189.
14. Giaume C, Leybaert L, Naus CC, Saez JC. Connexin and pannexin hemichannels in brain glial cells: properties, pharmacology, and roles. *Front Pharmacol* 2013; **4**: 88.
15. MacVicar BA, Thompson RJ. Non-junction functions of pannexin-1 channels. *Trends Neurosci* 2010; **33**: 93–102.
16. Orellana JA, von Bernhardi R, Giaume C, Saez JC. Glial hemichannels and their involvement in aging and neurodegenerative diseases. *Rev Neurosci* 2012; **23**: 163–177.
17. Davidson JO, Green CR, Bennet L, Nicholson LF, Danesh-Meyer H, O'Carroll SJ *et al.* A key role for connexin hemichannels in spreading ischemic brain injury. *Curr Drug Targets* 2013; **14**: 36–46.
18. Chen G, Park CK, Xie RG, Berta T, Nedergaard M, Ji RR. Connexin-43 induces chemokine release from spinal cord astrocytes to maintain late-phase neuropathic pain in mice. *Brain* 2014; **137**(Pt 8): 2193–2209.
19. Retamal MA, Froger N, Palacios-Prado N, Ezan P, Saez PJ, Saez JC *et al.* Cx43 hemichannels and gap junction channels in astrocytes are regulated oppositely by proinflammatory cytokines released from activated microglia. *J Neurosci* 2007; **27**: 13781–13792.
20. Karpuk N, Burkovetskaya M, Fritz T, Angle A, Kielian T. Neuroinflammation leads to region-dependent alterations in astrocyte gap junction communication and hemichannel activity. *J Neurosci* 2011; **31**: 414–425.
21. Orellana JA, Shoji KF, Abudara V, Ezan P, Amigou E, Saez PJ *et al.* Amyloid beta-induced death in neurons involves glial and neuronal hemichannels. *J Neurosci* 2011; **31**: 4962–4977.
22. Abudara V, Roux L, Dallerac G, Matias I, Dulong J, Mothet JP *et al.* Activated microglia impairs neuroglial interaction by opening Cx43 hemichannels in hippocampal astrocytes. *Glia* 2015; **63**: 795–811.

23. Delekate A, Fuchtemeier M, Schumacher T, Ulbrich C, Foddis M, Petzold GC. Metabotropic P2Y1 receptor signalling mediates astrocytic hyperactivity in vivo in an Alzheimer's disease mouse model. *Nat Commun* 2014; **5**: 5422.
24. Jankowsky JL, Slunt HH, Ratovitski T, Jenkins NA, Copeland NG, Borchelt DR. Co-expression of multiple transgenes in mouse CNS: a comparison of strategies. *Biomol Eng* 2001; **17**: 157–165.
25. Giaume C, Orellana JA, Abudara V, Saez JC. Connexin-based channels in astrocytes: how to study their properties. *Methods Mol Biol* 2012; **814**: 283–303.
26. Kim HS, Suh YH. Minocycline and neurodegenerative diseases. *Behav Brain Res* 2009; **196**: 168–179.
27. De Vuyst E, Wang N, Decrock E, De Bock M, Vinken M, Van Moorhem M *et al.* Ca(2+) regulation of connexin 43 hemichannels in C6 glioma and glial cells. *Cell Calcium* 2009; **46**: 176–187.
28. Kuchibhotla KV, Lattarulo CR, Hyman BT, Bacskai BJ. Synchronous hyperactivity and intercellular calcium waves in astrocytes in Alzheimer mice. *Science* 2009; **323**: 1211–1215.
29. Ma T, Du X, Pick JE, Sui G, Brownlee M, Klann E. Glucagon-like peptide-1 cleavage product GLP-1(9-36) amide rescues synaptic plasticity and memory deficits in Alzheimer's disease model mice. *J Neurosci* 2012; **32**: 13701–13708.
30. Meyer-Luehmann M, Spires-Jones TL, Prada C, Garcia-Alloza M, de Calignon A, Rozkalne A *et al.* Rapid appearance and local toxicity of amyloid-beta plaques in a mouse model of Alzheimer's disease. *Nature* 2008; **451**: 720–724.
31. Hu X, Shi Q, Zhou X, He W, Yi H, Yin X *et al.* Transgenic mice overexpressing reticulon 3 develop neuritic abnormalities. *EMBO J* 2007; **26**: 2755–2767.
32. Contreras JE, Sanchez HA, Eugenin EA, Speidel D, Theis M, Willecke K *et al.* Metabolic inhibition induces opening of unapposed connexin 43 gap junction hemichannels and reduces gap junctional communication in cortical astrocytes in culture. *Proc Natl Acad Sci USA* 2002; **99**: 495–500.
33. Froger N, Orellana JA, Calvo CF, Amigou E, Kozoriz MG, Naus CC *et al.* Inhibition of cytokine-induced connexin43 hemichannel activity in astrocytes is neuroprotective. *Mol Cell Neurosci* 2010; **45**: 37–46.
34. Iglesias R, Dahl G, Qiu F, Spray DC, Scemes E. Pannexin 1: the molecular substrate of astrocyte "hemichannels". *J Neurosci* 2009; **29**: 7092–7097.
35. Busche MA, Eichhoff G, Adelsberger H, Abramowski D, Wiederhold KH, Haass C *et al.* Clusters of hyperactive neurons near amyloid plaques in a mouse model of Alzheimer's disease. *Science* 2008; **321**: 1686–1689.
36. Silverman WR, de Rivero Vaccari JP, Locovei S, Qiu F, Carlsson SK, Scemes E *et al.* The pannexin 1 channel activates the inflammasome in neurons and astrocytes. *J Biol Chem* 2009; **284**: 18143–18151.
37. Parvathenani LK, Tertyshnikova S, Greco CR, Roberts SB, Robertson B, Posmantur R. P2X7 mediates superoxide production in primary microglia and is up-regulated in a transgenic mouse model of Alzheimer's disease. *J Biol Chem* 2003; **278**: 13309–13317.
38. Alberdi E, Wyssenbach A, Alberdi M, Sanchez-Gomez MV, Cavaliere F, Rodriguez JJ *et al.* Ca(2+) -dependent endoplasmic reticulum stress correlates with astrogliosis in oligomeric amyloid beta-treated astrocytes and in a model of Alzheimer's disease. *Aging Cell* 2013; **12**: 292–302.
39. Grolla AA, Fakhfouri G, Balzaretti G, Marcello E, Gardoni F, Canonico PL *et al.* Abeta leads to Ca(2)(+) signaling alterations and transcriptional changes in glial cells. *Neurobiol Aging* 2013; **34**: 511–522.
40. De Bock M, Wang N, Bol M, Decrock E, Ponsaerts R, Bultynck G *et al.* Connexin 43 hemichannels contribute to cytoplasmic Ca2+ oscillations by providing a bimodal Ca2+-dependent Ca2+ entry pathway. *J Biol Chem* 2012; **287**: 12250–12266.
41. Ye ZC, Wyeth MS, Baltan-Tekkok S, Ransom BR. Functional hemichannels in astrocytes: a novel mechanism of glutamate release. *J Neurosci* 2003; **23**: 3588–3596.
42. Stridh MH, Tranberg M, Weber SG, Blomstrand F, Sandberg M. Stimulated efflux of amino acids and glutathione from cultured hippocampal slices by omission of extracellular calcium: likely involvement of connexin hemichannels. *J Biol Chem* 2008; **283**: 10347–10356.
43. Stout CE, Costantin JL, Naus CC, Charles AC. Intercellular calcium signaling in astrocytes via ATP release through connexin hemichannels. *J Biol Chem* 2002; **277**: 10482–10488.
44. Kang J, Kang N, Lovatt D, Torres A, Zhao Z, Lin J *et al.* Connexin 43 hemichannels are permeable to ATP. *J Neurosci* 2008; **28**: 4702–4711.
45. Jo S, Yarishkin O, Hwang YJ, Chun YE, Park M, Woo DH *et al.* GABA from reactive astrocytes impairs memory in mouse models of Alzheimer's disease. *Nat Med* 2014; **20**: 886–896.
46. Talantova M, Sanz-Blasco S, Zhang X, Xia P, Akhtar MW, Okamoto S *et al.* Abeta induces astrocytic glutamate release, extrasynaptic NMDA receptor activation, and synaptic loss. *Proc Natl Acad Sci USA* 2013; **110**: E2518–E2527.
47. Kuchibhotla KV, Goldman ST, Lattarulo CR, Wu HY, Hyman BT, Bacskai BJ. Abeta plaques lead to aberrant regulation of calcium homeostasis in vivo resulting in structural and functional disruption of neuronal networks. *Neuron* 2008; **59**: 214–225.
48. Lin MT, Beal MF. Mitochondrial dysfunction and oxidative stress in neurodegenerative diseases. *Nature* 2006; **443**: 787–795.
49. Xie H, Hou S, Jiang J, Sekutowicz M, Kelly J, Bacskai BJ. Rapid cell death is preceded by amyloid plaque-mediated oxidative stress. *Proc Natl Acad Sci USA* 2013; **110**: 7904–7909.
50. Pelegrin P, Surprenant A. The P2X(7) receptor-pannexin connection to dye uptake and IL-1beta release. *Purinergic Signal* 2009; **5**: 129–137.
51. Erb L, Cao C, Ajit D, Weisman GA. P2Y receptors in Alzheimer's disease. *Biol Cell* 2015; **107**: 1–21.
52. Fujita T, Tozaki-Saitoh H, Inoue K. P2Y1 receptor signaling enhances neuroprotection by astrocytes against oxidative stress via IL-6 release in hippocampal cultures. *Glia* 2009; **57**: 244–257.
53. Jimenez S, Torres M, Vizuete M, Sanchez-Varo R, Sanchez-Mejias E, Trujillo-Estrada L *et al.* Age-dependent accumulation of soluble amyloid beta (Abeta) oligomers reverses the neuroprotective effect of soluble amyloid precursor protein-alpha (sAPP(alpha)) by modulating phosphatidylinositol 3-kinase (PI3K)/Akt-GSK-3beta pathway in Alzheimer mouse model. *J Biol Chem* 2011; **286**: 18414–18425.
54. Delarasse C, Auger R, Gonnord P, Fontaine B, Kanellopoulos JM. The purinergic receptor P2X7 triggers alpha-secretase-dependent processing of the amyloid precursor protein. *J Biol Chem* 2011; **286**: 2596–2606.
55. Durand D, Carniglia L, Beauquis J, Caruso C, Saravia F, Lasaga M. Astroglial mGlu3 receptors promote alpha-secretase-mediated amyloid precursor protein cleavage. *Neuropharmacology* 2014; **79**: 180–189.
56. Cotrina ML, Gao Q, Lin JH, Nedergaard M. Expression and function of astrocytic gap junctions in aging. *Brain Res* 2001; **901**: 55–61.
57. Nimmerjahn A, Kirchhoff F, Kerr JN, Helmchen F. Sulforhodamine 101 as a specific marker of astroglia in the neocortex in vivo. *Nat Methods* 2004; **1**: 31–37.
58. Hirase H, Qian L, Bartho P, Buzsaki G. Calcium dynamics of cortical astrocytic networks in vivo. *PLoS Biol* 2004; **2**: E96.
59. Fossat P, Turpin FR, Sacchi S, Dulong J, Shi T, Rivet JM *et al.* Glial D-serine gates NMDA receptors at excitatory synapses in prefrontal cortex. *Cereb Cortex* 2012; **22**: 595–606.
60. Shi Q, Hu X, Prior M, Yan R. The occurrence of aging-dependent reticulon 3 immunoreactive dystrophic neurites decreases cognitive function. *J Neurosci* 2009; **29**: 5108–5115.

Supplementary Information accompanies this paper on Cell Death and Differentiation website (http://www.nature.com/cdd)